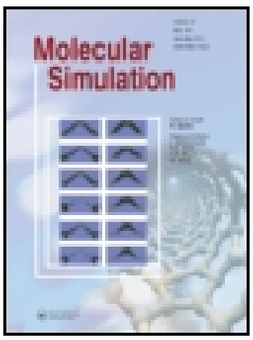

Molecular Simulation

ISSN: 0892-7022 (Print) 1029-0435 (Online) Journal homepage: http://www.tandfonline.com/loi/gmos20

Ice adhesion mechanism on lubricant-impregnated surfaces using molecular dynamics simulations

Atanu K. Metya & Jayant K. Singh

To cite this article: Atanu K. Metya & Jayant K. Singh (2018): Ice adhesion mechanism on lubricant-impregnated surfaces using molecular dynamics simulations, Molecular Simulation, DOI: 10.1080/08927022.2018.1513649

To link to this article: https://doi.org/10.1080/08927022.2018.1513649

Published online: 26 Aug 2018.

MOLECULAR SIMULATION
https://doi.org/10.1080/08927022.2018.1513649

Taylor & Francis
Taylor & Francis Group

Ice adhesion mechanism on lubricant-impregnated surfaces using molecular dynamics simulations

Atanu K. Metya and Jayant K. Singh

Department of Chemical Engineering, Indian Institute of Technology Kanpur, Kanpur, India

ABSTRACT

Ice formation causes numerous problems in many industrial fields as well as in our daily life. The control of ice nucleation and rational design of anti-icing surface with low ice adhesion are desirable in various industries such as aircraft, power line, ships, building, and cryopreservation. However, despite considerable attention in the development of ice or water-repellent surfaces, it is still challenging to design icephobic or anti-icing surfaces with high resistance to icing. In this study, coarse-grained molecular dynamics simulation is utilised to investigate the ice adhesion mechanism on lubricant-infused nanotextured surfaces. Using steered molecular dynamics simulation, we find that the adhesion strength of ice on nanotextured surfaces impregnated with lubricant films to be higher compared to that on textured surfaces in presence excess lubricant films. We illustrate that the ice adhesion strength depends on the texture density and the ice adhesion strength increases with nanoposts density. Lubricant-impregnated surfaces (LISs) with higher posts density exhibit greater adhesive interaction energy due to the large contact area between the icecube and the textured surface. This systematic study enhances our understanding of ice adhesion mechanism on LISs which can apply for designing novel anti-icing surfaces with extremely weak ice adhesion strength.

ARTICLE HISTORY
Received 22 April 2018
Accepted 10 August 2018

KEYWORDS
Ice adhesion; lubricant-impregnated surfaces; coarse-grained; steered molecular dynamics

1. Introduction

Ice formation and accumulation on solid surfaces play a significant role in various industries. It can cause a serious problem in the performance of wind turbines, solar panels and reduce the offshore operational safety [1–3]. In some cases, excessive ice build-up leads to crash of aircraft, collapse of building and transmission line, which result in severe economic loss [4–6]. Several traditional anti-icing and de-icing methods have been developed and widely applied to remove accumulated snow, ice or frost which are based on thermal treatments, mechanical removal, and chemical modifications. These methods are costly and environmentally harmful. In addition, they are also inefficient for protection from ice build-up for longer duration [1,7,8]. Therefore, materials that can inhibit ice formation and accumulation for long-term usage in industrial and technological applications is essential. The idea of developing anti-icing surfaces should be that which promote the freezing delay and reduced the adhesion of ice to these surfaces so that accumulated ice can be easily removed merely under natural actions (e.g. gravity or wind). Thus, the underlying mechanism needs to be known for an understanding of heterogeneous nucleation of ice.

Over the last several years, superhydrophobic surfaces have been considered to be a promising material for preventing ice formation. Superhydrophobicity is generally achieved by introducing surface textures in different length scales and use of low surface energy coating. A large number of investigations have shown the anti-icing and de-icing performance of superhydrophobic surfaces [8–21]. Superhydrophobic surfaces exhibit delay in ice formation [22–25] and reduce the solid–liquid contact time of an impacting water droplet [26–31]. The delay or shorter contact time allow water droplet to detach spontaneously from the superhydrophobic surfaces before the droplet freeze. Furthermore, a surface with a lower ice adhesion strength is considered to have good ice-repellent properties [10, 12,32,33]. However, superhydrophobic surfaces lose their water or ice repellent abilities when the water adsorption and condensation occur or ice covers the whole surface textures [13,34–37]. Varanasi et al. [38] reported that frost formation within the textures of superhydrophobic surfaces under the subzero condition and found higher ice adhesion than that on the smooth surfaces. This could be because of wetting transition from the Cassie state to the Wenzel state of water droplets during the freezing process on the textured surfaces [34]. Therefore, condensed and impacting water droplet can form 'Wenzel ice' [12], which leads to the mechanical interlock and consequently the interfacial area between ice and the textured surface is substantially enhanced [12,34].

In order to address the aforementioned problems for ice formation on superhydrophobic surfaces, recently a great effort has been made for the rational design of water or ice repellent surfaces by incorporating a water-immiscible organic liquid in a porous material or textured surface [39–41]. In this new approach to superhydrophobicity, slippery liquid-infused porous surfaces (SLIPS) [42–44]and lubricant-impregnated surfaces (LISs) [45–47] were developed. Here, an immiscible liquid layer acts as a lubricant, which is trapped between the substrate surface and the ice, and consequently provides a

CONTACT Jayant K. Singh jayantks@iitk.ac.in

very weak interaction between the substrate and the ice. These surfaces have recently attracted tremendous attention for anti-icing and de-icing because of their remarkable slippery properties. Numerous studies have shown that various lubricant-infused textured surfaces provide remarkable low ice adhesion, repel a variety of simple and complex liquids, exhibit self-cleaning and very low droplet roll-off properties [42, 44, 47–49]. Kim et al. [43] reported that the ice adhesion strength of SLIPS with excess lubricant is reduced by a 1–2 order of magnitude compared to any conventional materials. Recently, Subramanyam et al. [50] investigated the effect of lubricant level in the LISs with micro-scale texture on ice adhesion and found higher ice adhesion on an LIS with an equilibrium film (i.e. no excess lubricant) compared to an LIS with an excess lubricant. Furthermore, the authors studied the dependence of ice adhesion on surface texture density (micro-scale textures) in presence of equilibrium film in the LIS and found that ice adhesion reduces with increasing texture density. This result is surprising because of an increase in interfacial contact area between the ice and the substrate with an increase in texture density, and consequently results in lower the ice adhesion strength. The authors demonstrate that the ice fractures increase with texture densities due to more defect or crack initiation sites at the edges of microposts which resulted in reducing ice adhesion [50]. Kim et al. studied the effect of micro-, nano-scale and hierarchy of surface topography on the stability of lubricant under the high shear condition and found that SLIPS with nano-scale uniform texture surfaces provide better liquid-repellent properties compared to the hierarchically structured surfaces at a strong shear condition. These experimental investigations are promising; however, the effect of nano-scale texture density on ice adhesion is not well study.

Here, we report direct computational evidence of ice adhesion on lubricant-impregnated texture surfaces using molecular dynamics simulations. The aim of this study is to provide the molecular level understanding of the ice–substrate interface in the ice adhesion mechanism using the coarse-grained model of water and lubricant. In this study, we use a fluorinated liquid as a lubricant, which is impregnated in a nano-scale texture surface with and without excess lubricant film. Furthermore, we study the effect of nano-pillar density on ice adhesion properties of LIS in absence of excess lubricant films.

2. Model and simulation details

In this work, water is modelled with the coarse-grained potential (i.e. monatomic water model mW) [51, 52]. This water model was reported to reproduce the structural, thermodynamical properties of ice and water, and has been extensively applied to study the crystallisation of bulk water and nanodroplets as well as on different substrates [53–64]. We create nano-textured surfaces using model graphite surface. The interaction parameters between the mW water and the atoms of graphite are adopted from the work of Lupi et al. [55] which is based on the parametrisation of the two-body term of the Stillinger–Weber (SW) potential, so that it can reproduce the macroscopic contact angle of water on a smooth graphite surface. Recent, experimental studies have shown that texture surfaces infused with a low surface energy perfluorinated oils exhibit noticeable ice-repellent properties [42–44, 50]. Therefore, in the present study, we have considered perfluorotri-*n*-pentylamine as a lubricant (fluorocarbon FC70), which is infused in the nanotextured surfaces. The perfluorotri-*n*-pentylamine molecules are described by the united-atom model. Lennard-Jones (LJ) 12-6 potential is used to describe non-bonded interaction for the CF_3, CF_2 and N fragments of the fluorocarbon molecules [65] with a cut-off of 1.4 nm. The bond, angle, and dihedral parameters are taken from the OPLS/AMBER force fields [66–68]. The non-bonded and bonded parameters are listed in Table 1. We have evaluated the density and liquid–vapour surface tension at 300 K and compared with the available literature values (Table 2). These simulated results are in line with the experimental values (within the error bar). The surface tension is computed from the normal P_N and tangential P_T components of the pressure using the mechanical expression [69, 70]:$\gamma = (L_z/2)[\langle P_N\rangle - \langle P_T\rangle]$.

The interaction between fluorocarbon (FC) lubricant and the mW water is modelled through 12-6 LJ potential. We employ the procedure of Qiu et al. [64, 71] to parameterise the interaction parameters so that the interfacial tension of water-lubricant due to the model matches the experimental value. The interfacial tension of water-fluorocarbon is computed from the pressure tension components using the mechanical definition as used for surface tension calculation [72]. The system contains 300 fluorocarbon molecules and 7000 mW water. The x- and y-dimensions of the simulation box are kept fixed (i.e. 6 nm × 6 nm). The simulation is conducted in the NP_zT ensemble, where the pressure is applied in the z-direction. The temperature (300 K) and pressure (1 atm) are controlled with the Nosé–Hoover thermostat and barostat, with a relaxation time of 1.0 and 10.0 ps, respectively. A periodic boundary condition is applied in all directions. The simulated lubricant-water interfacial tension at 300 K, without

Table 1. Perfluorotri-*n*-pentylamine force field parameters [65–68].

Species	σ (Å)	ε (kcal mol^{-1})	
CF_3	4.65	0.1987	
CF_2	4.65	0.0596	
N	3.25	0.1700	
Bonds	r_0 (Å)	K_r (kcal mol^{-1} Å^{-2})	
CF_3–CF_2	1.529	268	
CF_2–N	1.448	382	
Angles	θ_0 (deg)	K_θ (kcal mol^{-1} rad^{-2})	
CF_3–CF_2–CF_2	58.35	112.70	
CF_2–CF_2–N	56.20	109.47	
CF_2–N–CF_2	51.80	107.20	
Dihedrals	V_1 (kcal mol^{-1})	V_2 (kcal mol^{-1})	V_3 (kcal mol^{-1})
CF_3/CF_2–CF_2–CF_2–CF_2	1.740	−0.157	0.279
CF_2–CF_2–CF_2–N	2.392	−0.674	0.550
CF_2–CF_2–N–CF_2	0.416	−0.128	0.695

Table 2. Density and liquid–vapour surface tensions of perfluorotri-*n*-pentylamine in MD simulations and in experiments.

Property	Simulations	Experiments
Density (kg m^{-3})	2019 ± 10	1940[a]
Surface tension (mN m^{-1})	14.2 ± 2.1	17.1 ± 0.3[b]

[a]At 298 K [42].
[b]At 295–297 K [42].

Table 3. Lennard-Jones (LJ) parameters between FC and mW water; and FC and graphite.

Species	Species	σ (Å)	ε (kcal mol^{-1})
CF_3	mW	3.908	0.1756
CF_2	mW	3.908	0.0962
N	mW	3.208	0.1624
CF_3	C	4.025	0.1052
CF_2	C	4.025	0.0576
N	C	3.325	0.0973

long-range correction, is found to be 55.8 $\pm$ 2.2 mN/m, which is in good agreement with the experimental value (56.1 $\pm$ 0.9 mN/m at 296–298 K) [42]. Furthermore, we have evaluated the contact angle [73, 74] of mW water on a lubricant surface, the simulation value of 119 $\pm$ 3° at 300 K is greater than the experimental value (113° at 293–298 K) [42]. The non-bonded interaction between graphite surface and the lubricant is described by 12-6 LJ potential. The interaction parameters are calculated according to the Lorentz–Berthelot mixing rules by considering the OPLS parameters of graphite carbon atom [75]. All the parameters are listed in Table 3. Lubricant-impregnated nanotextured surface with and without excess lubricant films and the icecube on that surfaces are presented in Figure 1. In the case of LIS with excess lubricant, the thickness of the film is ~1.8 nm above the top of the pillar. For LIS without excess lubricant, the number of perfluorotri-*n*-pentylamine molecules are considered based on the effective volume available in the nanotextured graphitic surfaces using the bulk density of lubricant (evaluated from the present simulation). We designed nanotextured surfaces consisting of nanopost (2.09 nm × 1.99 nm and height of 2.04 nm) by varying inter-post spacing using model graphite surface. The textured surface consists of four atomic layers of graphene as a base layer and a post made out of additional graphite sheets on the top of the base layer.

The following simulation protocol is adopted. (1) First water film with a thickness of ~2.2 nm is placed on the LIS and equilibrate the system at 300 K. (2) Then, the system is cooled down to 180 K with a cooling ramp of 1 K/ns. (3) Finally, isothermal simulation is carried out at 180 K for 20 ns. This ice crystal on LIS is used to perform constant-velocity steered molecular dynamics (SMD) simulation at 180 K temperature to measure the ice adhesion of that surface. In the present investigation, the MD simulations are performed in the *NVT* ensemble using LAMMPS simulation package [76] Periodic boundary conditions of the simulation box are applied in the *x*- and *y*-directions and non-periodic in the *z*-direction with ~15 nm above the ice crystal in order to avoid interaction with its periodic surface and simulate the system with a free surface. The temperature in the MD simulations is controlled by Nosé–Hoover thermostat with a relaxation time of 1 ps and an integration time step of 5 fs. The atoms of LIS are kept fixed during the SMD simulations.

The adhesion strength of an ice crystal on the substrate is investigated by using SMD simulation approach [77–79]. In this simulation, time-dependent external forces are generated by an external harmonic potential. The harmonic spring potential can be expressed as

$$\mathcal{U}_{SMD}(t) = \frac{\mathcal{K}}{2}[vt - (Z(t) - Z_0)]^2 \tag{1}$$

where $\mathcal{K}$ is the spring constant, and Z_0 is the initial position of the centre of mass (COM) of an icecube moving with a constant velocity v in the pulling process. $Z(t)$ is the current position of the COM of icecube and the harmonic potential acting on the COM of the *z*-coordinate of icecube during the pulling process. The pulling force exerted on the COM of the icecube can be defined as

$$\mathcal{F}(t) = \mathcal{K}[vt - (Z(t) - Z_0)] \tag{2}$$

Within the framework of free energy landscape with respect to the chosen coordinate, the external work can be evaluated based on the given equation [80, 81]:

$$\mathcal{W}(t) = \int_0^t \mathcal{F} v \, dt \tag{3}$$

The free energy difference or the work done for separating the two states can be calculated based on the Jarzynski's equality [78], which provides an estimation of the potential mean force (PMF) from a nonequilibrium process using a good statistic for averaging [82]. According to Jarzynski's equality [78], the free energy ΔF can be estimated based on the following

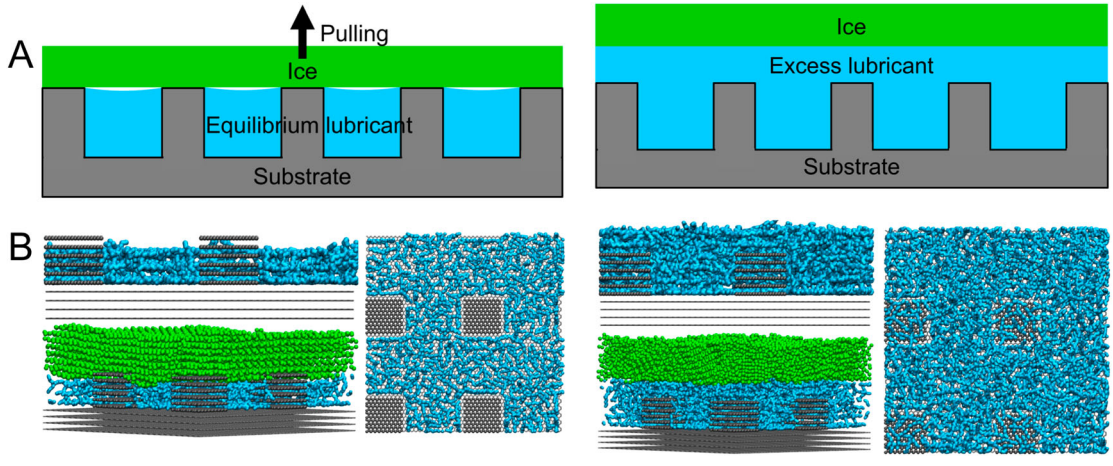

Figure 1. (Colour online) (A) Schematic illustration of a icecube subjected to pulling on LIS in presence (left) and absence (right) excess lubricant films. (B) Top and side views of simulation system: (left) with no excess and (right) with excess lubricant.

equation:

$$\Delta F = -\frac{1}{\beta}\log\langle\exp(-\beta\mathcal{W})\rangle \quad (4)$$

where $\beta = 1/(k_B T)$ in which k_B is Boltzmann constant and T is the temperature. $\mathcal{W}$ is the work during pulling or shearing process and $\langle\cdots\rangle$ denotes the ensemble average.

Recently, this force-probe MD simulation has been performed to investigate the detaching and shearing stress of icecube on silicon, graphene [83] and on single-walled carbon nanotubes array [84]. In the present study, the pulling or sliding velocity is constant and is considered to be 0.5 nm/ns. The force is either normal or parallel to the substrate for pulling and sliding of an icecube, respectively, and the spring constant K is chosen to be 1.2 kcal/mol/nm^2 in accordance with a previous investigation [83]. We have performed at least 6 independent SMD runs after equilibrium to estimate the ice adhesion strength.

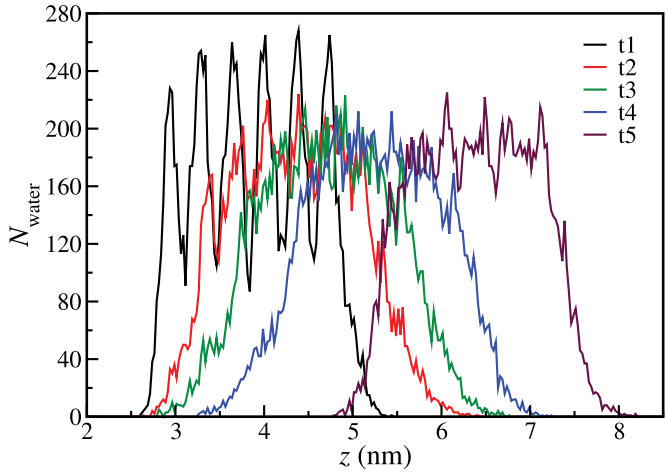

Figure 3. (Colour online) The number of water molecules as a function of distance z above the surface (post density, $\varphi_p = 4 \times 10^{15}/\text{m}^2$) during pulling at different times (i.e. t1 < t2 < t3 < t4 < t5).

3. Results and discussions

We first examine how the ice adhesion is influenced by the lubricant film. The ice adhesion strength obtained from pulling the icecube off the substrate perpendicular to the ice–substrate interfacial plane at 180 K. Figure 2 illustrates the pulling force onto the COM of the icecube as a function of pulling distance during the SMD simulations with a pulling rate of 0.5 nm/ns and a sequential snapshot during pulling process of a typical SMD simulation. We find that during the pulling process the icecube is first pulled at one corner from the LIS and then detached completely from that substrate. A similar behaviour has seen earlier MD study of ice adhesion on smooth graphene and silicon surfaces [83]. Figure 3 shows the number of water molecules as a function of distance along the direction normal to the substrate during the pulling process. The decrease in ordered peaks height in the density profile appears due to tilting of the icecube as the pulling force reaches to maximum pulling force (see snapshots b and c in Figure 2). The density profile also supports that the icecube is pulled at one corner from the LIS (i.e. at t2, t3, t4) and then detached completely from that substrate (at t5) during the detachment process of the icecube. The detaching force is obtained from the maximum force at which a sudden drop in the force-distance profiles. The pulling strength or detaching stress is evaluated by taking the maxima of the pulling force ($\mathcal{F}_{pull}^{max}$) divided by interfacial area (A). We have also observed the pulling force increases as applied velocity becomes larger. Figure 4 shows the ice adhesion strength toLIS (post density, $\varphi_p = 28 \times 10^{15}/\text{m}^2$) in presence and absence of the excess lubricant films. The average detaching stress to LIS with excess lubricant films is lower than that on LIS without excess lubricant films. In experiments, the ice

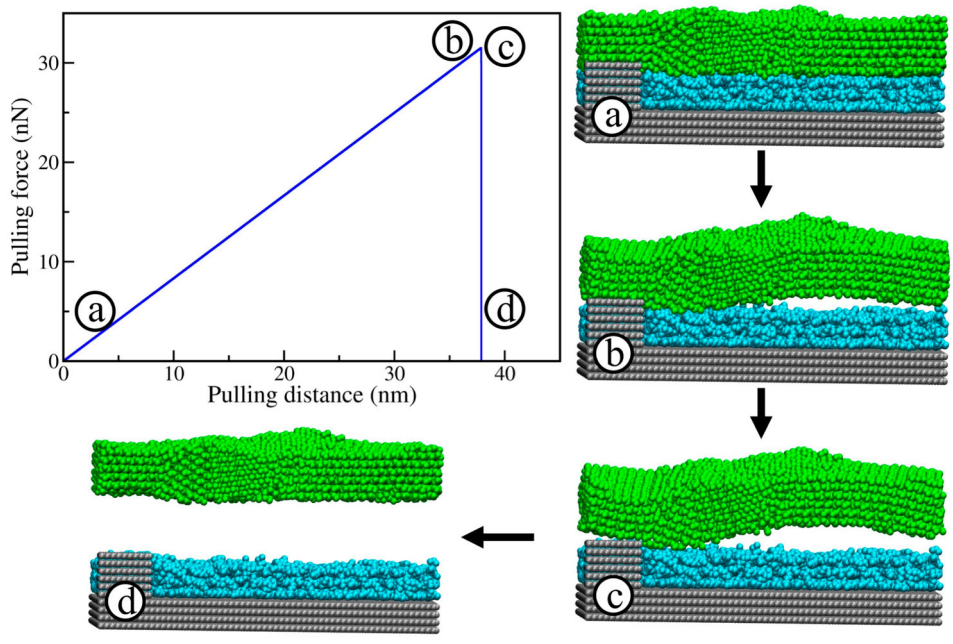

Figure 2. (Colour online) Pulling force loaded on the COM of the icecube as a function of pulling distance $Z(t)$ at a constant pulling rate.

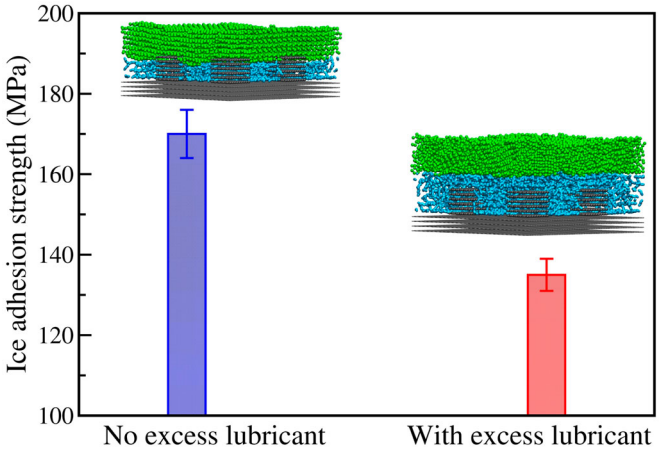

Figure 4. (Colour online) Comparison of the average ice adhesion strength (i.e. detaching stress) on LIS with and without excess lubricant films.

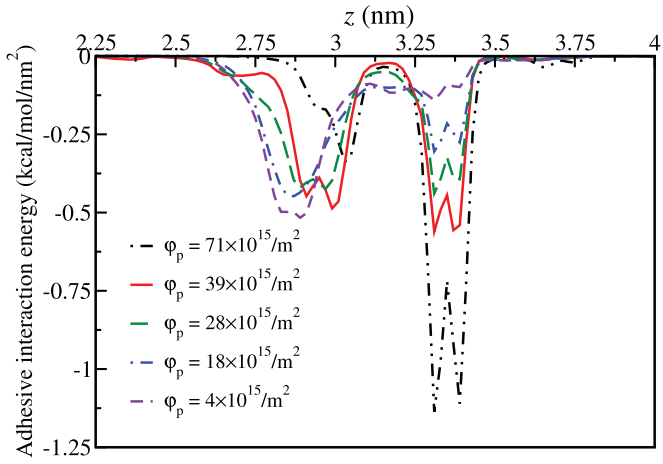

Figure 6. (Colour online) Plot of adhesive energy along the orthogonal direction to the LIS for different nanopost density.

adhesion strength on superhydrophobic surfaces is less than 2.5 MPa [48, 85], which is two order of magnitude lower than the computed adhesive strength using SMD simulations [83, 84]. This high value of strength arises due to high pulling rate applied in SMD simulations, which is ≈ 6–7 orders of magnitude higher compared to experimental rate [83]. Subramanyam et al. [50] investigated the lubricant film dependent ice adhesion strength on LIS and found that about 15 times lower ice adhesion on LIS with excess lubricant (silicon oil and DC704) than that of texture surfaces without excess films. In this study, we used perfluorotri-*n*-pentylamine as a lubricant and found that the detaching stress of an icecube on LIS with excess lubricant is 135 ± 4 MPa, which is ∼20% lower than on that LIS ($\varphi_p = 28 \times 10^{15}/m^2$) without excess films. In addition, we evaluate the crystallisation temperature of the water film on LIPs with and without excess lubricant. We have performed 6–8 independent simulations with a cooling rate of 0.5 K/ns and each starting at a temperature of 240 K. In these simulations, lubricant molecules are kept unfrozen. The crystallisation temperatures obtained for LIPs ($\varphi_p = 28 \times 10^{15}/m^2$) without and with excess lubricant are 203 ± 2 K and 193 ± 2 K, respectively. Therefore, in the presence of excess films, the hydrophobicity of the substrate is enhanced than that of LIS without excess lubricant films and as a consequence higher value of the ice adhesion strength. This is consistent with the observed lower value of crystallisation temperature of water on LIS with excess lubricant compared to a lubricant-infused textured surface without excess lubricant.

Next, we investigate the effect of nanoposts density on ice adhesion by varying the spacing between the posts. Figure 5 (a) shows the pulling force observed during the SMD simulations of detaching icecube for different post density in the LIS. The average adhesion strength of ice (i.e. normalised by that on smooth graphite substrate surface) obtained from the pulling process is plotted in Figure 5(b). We find that ice adhesion strength is dependent on texture and increases with increase in the density of nanoposts. We observe that at lower values of texture density, the ice adhesion strength increases linearly with increase in texture density. Experimental investigations have shown that the ice adhesion strength on the textured surface increases with an increase in the total ice–substrate contact area [34, 38]. Meuler et al. [12] found that the average ice adhesion strength correlates linearly with the practical work of adhesion for the liquid water drop on bare steel and different coatings surfaces. In this work, the results are in line with the experimental observation i.e. as the nanopost density increases, the ice–solid

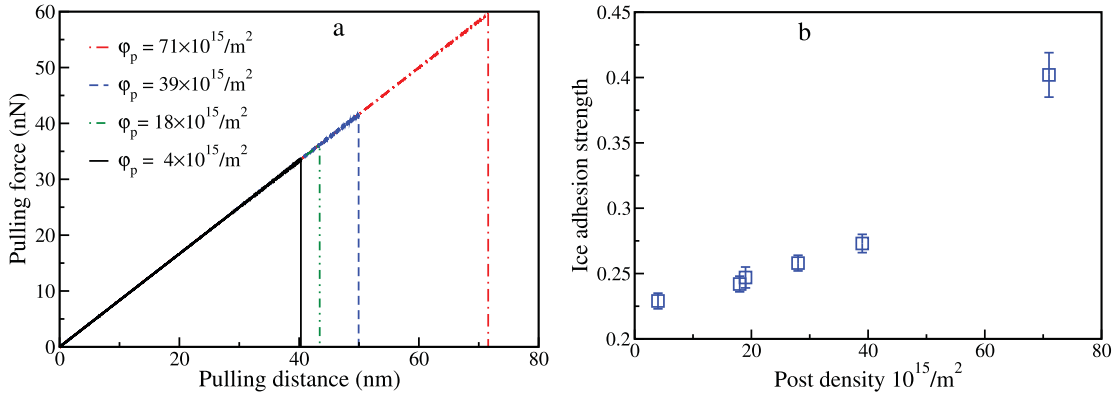

Figure 5. (Colour online) (a) Plot of the pulling force as a function of pulling distance during detachment of the icecube from the LIPs. (b) The average ice adhesion strength normalised by that on smooth graphite substrate surface as a function of nanoposts density.

Table 4. Adhesive interaction energy and adhesion strength (from PMF) of icecube for different LISs.

Post density $\times 10^{15}/m^2$	Adhesive interaction energy (kcal/nm^2)	Adhesion energy (mJ/m^2)
71	-9.90 ± 0.07	0.517
39	-9.04 ± 0.15	0.265
28	-8.74 ± 0.17	0.234
18	-8.48 ± 0.10	0.214
4	-8.10 ± 0.06	0.177

(texture) contact area is enhanced leading to increase in the ice adhesion strength on LIS. However, Subramanyam et al. [50] have shown that ice adhesion strength enhances with decreasing the density of microposts, which is counter-intuitive because the highest ice–solid substrate contact area in their work performed the best anti-icing surface. The authors argued that ice adhesion strength is reduced due to the brittle adhesive failure at the ice–solid interface which indicates the high-density stress and cracks initiate sites at the edges of the microposts of the lubricant-impregnated microtextured surfaces [50].

We also evaluated the adhesive interaction energy between the LISs and the icecube along the normal to the substrate surface as shown in Figure 6. Here the icecube interacts with substrate surface through the van der Waals (vdW) interaction. The first trough appears in the range of ~2.7–3.1 nm due to the presence of water molecules below the top of the pillar surface (z=3.1 nm, the centre position of the top of the texture graphite substrate surface). The second trough clearly indicates that the interaction energy between the icecube and the substrate increases with an increase in post density. As the texture density increases the contact area between the posts and the icecube is increased, and as a consequence higher value interaction between an icecube and a lubricant-infused texture surface. We evaluate total adhesive interaction energy per unit area for different LISs (see Table 4) which are consistent with the ice adhesion strength obtained from the pulling process. Furthermore, we have calculated the adhesion energy of icecube from the potential mean force and found that the adhesion energy enhances with an increase in nanopost density.

In order to understand the ice shearing mechanism on LIS, we apply a constant shearing rate onto the COM of the icecube parallel to the substrate (i.e. x-direction of the simulation system.) In order to move the icecube on LIS, we increase the surface area in x-direction 3 times and 2 times in y-direction of the original simulation boxes, as shown by the simulation snapshot in Figure 7. Figure 7 also shows the shearing force curve obtained as a function of the sliding distance for a nanopost density of 28×10^{15}. A similar shearing behaviour of an icecube on LIS without excess lubricant films is observed during the sliding process for all other systems, which is consistent with a previous force-probe MD study [83]. To address the effect on the density profile in the shearing process of the icecube, we plot the average number of water molecules as a function of distance along the direction normal to the substrate during sliding of icecube at different times as shown in Figure 8. From the density profile, it is clear that after the first sliding of the icecube (i.e. maximum force in Figure 7), the crystal structure of the icecube is slightly distorted, though negligible as tetrahedral order parameter (figure not given) indicates no significant change in the ice structure. We evaluate the shearing stress from the maximum force required to move the icecube on the LIS and the average shearing stress is 25 ± 3 MPa, which is about 7 times lower than the detaching stress on the lubricant-impregnated nanotextured surface. We observe that the effect of nanopost density on the ice shearing on LIPs is less sensitive and the average shearing stress varies in the range of ~23–30 MPa with nanopost density.

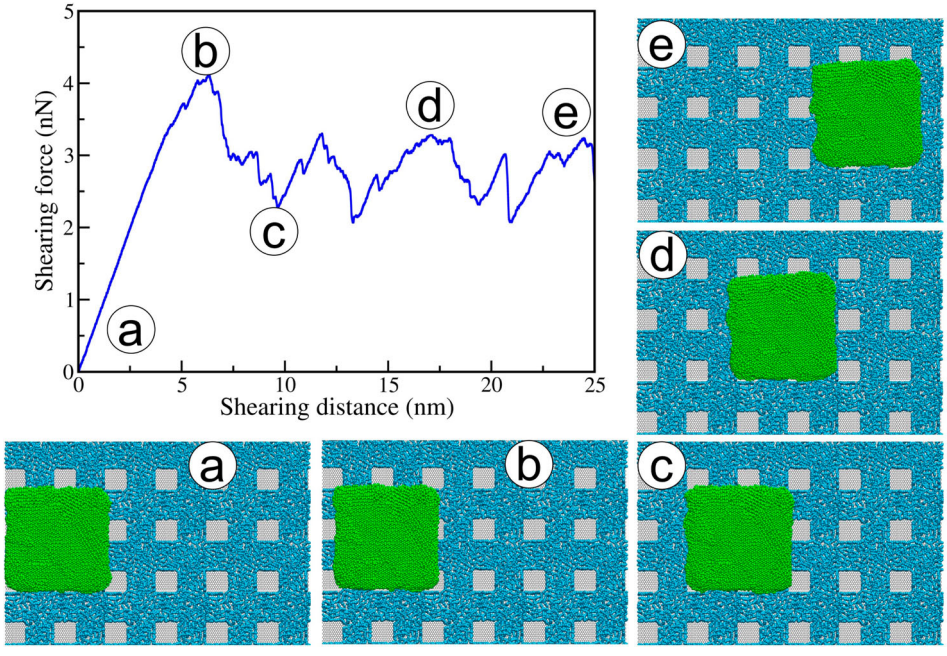

Figure 7. (Colour online) The shearing force as a function of shearing distance. Snapshots (a–e) show the icecube at different position on the LIS during sliding.

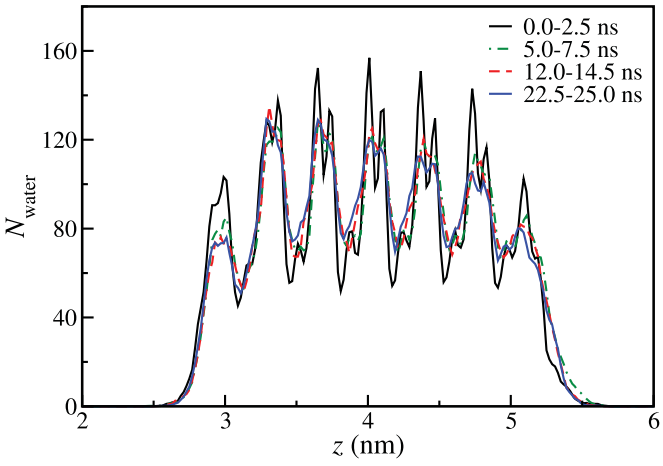

Figure 8. (Colour online) Average number of water molecules as a function of distance z above the surface during sliding of the icecube (post density, $\varphi_p = 28 \times 10^{15}/m^2$).

4. Conclusions

We have systematically performed the coarse-grained model of water and lubricant to simulate the ice adhesion mechanism on lubricant-impregnated textured surfaces using SMD simulations. We find that the lower adhesion strength of the icecube on LIS with excess lubricant layer than the LIS in absence of excess lubricant films. By varying the density of nanoposts in the LISs, we show that the ice adhesion strength (i.e. detaching stress) depends on the texture density and increases with nanoposts density. This is mainly due to the increase in the ice–solid contact area which explains the increasing trends in the ice adhesion on LIS. We find that the adhesive interaction between the icecube and the solid substrate surface increases with nanopost density. However, our molecular level investigation does not provide an explanation for the experimental observations of ice adhesion on LISs on square microposts with micro-scale inter-post spacing [50], where ice adhesion strength is reported to minimise by the number of crack initiation sites in the LIS. Furthermore, we study the shearing of icecube on LIS which is found to be less sensitive with variation in the nanopost density.

Acknowledgements

The computational resources are provided by the High Performance Computing facilities of Indian Institute of Technology Kanpur.

Disclosure statement

No potential conflict of interest was reported by the authors.

Funding

This work is supported by the Department of Science and Technology (DST), Government of India.

References

[1] Laforte J, Allaire M, Laflamme J. State-of-the-art on power line de-icing. Atmos Res. 1998;46:143–158. Available from: http://www.sciencedirect.com/science/article/pii/S0169809597000574

[2] Dalili N, Edrisy A, Carriveau R. A review of surface engineering issues critical to wind turbine performance. Renew Sustain Energy Rev. 2009;13:428–438. Available from: http://www.sciencedirect.com/science/article/pii/S1364032107001554

[3] Ryerson CC. Ice protection of offshore platforms. Cold Reg Sci Technol. 2011;65:97–110. Anti-Icing and De-Icing Techniques; Available from: http://www.sciencedirect.com/science/article/pii/S0165232X10000327

[4] Lynch FT, Khodadoust A. Effects of ice accretions on aircraft aerodynamics. Prog Aerosp Sci. 2001;37:669–767. Available from: http://www.sciencedirect.com/science/article/pii/S0376042101000185

[5] Farzaneh M. Ice accretions on high-voltage conductors and insulators and related phenomena. Philos Trans R Soc Lond A, Math Phys Eng Sci. 2000;358:2971–3005. Available from: http://rsta.royalsocietypublishing.org/content/358/1776/2971

[6] Farzaneh M, Volat C, Leblond A. Anti-icing and de-icing techniques for overhead lines. Dordrecht, Netherlands: Springer; 2008. p. 229–268.

[7] Ramakrishna DM, Viraraghavan T. Environmental impact of chemical deicers – a review. Water Air Soil Pollut. 2005 Sep;166:49–63. Available from: https://doi.org/10.1007/s11270-005-8265-9

[8] Lv J, Song Y, Jiang L, et al. Bio-inspired strategies for anti-icing. ACS Nano. 2014;8:3152–3169. pMID: 24592934; Available from: http://dx.doi.org/10.1021/nn406522n

[9] Cao L, Jones AK, Sikka VK, et al. Anti-icing superhydrophobic coatings. Langmuir. 2009;25:12444–12448. pMID: 19799464; Available from: http://dx.doi.org/10.1021/la902882b

[10] Kulinich S, Farzaneh M. Ice adhesion on super-hydrophobic surfaces. Appl Surf Sci. 2009;255:8153–8157. Available from: http://www.sciencedirect.com/science/article/pii/S0169433209006369

[11] Tourkine P, Le Merrer M, Quéré D. Delayed freezing on water repellent materials. Langmuir. 2009;25:7214–7216. Available from: http://dx.doi.org/10.1021/la900929u

[12] Meuler AJ, McKinley GH, Cohen RE. Exploiting topographical texture to impart icephobicity. ACS Nano. 2010;4:7048–7052. Available from: http://dx.doi.org/10.1021/nn103214q

[13] Jung S, Dorrestijn M, Raps D, et al. Are superhydrophobic surfaces best for icephobicity? Langmuir. 2011;27:3059–3066. Available from: http://dx.doi.org/10.1021/la104762g

[14] Yao X, Song Y, Jiang L. Applications of bio-inspired special wettable surfaces. Adv Mater. 2011;23:719–734. Available from: http://dx.doi.org/10.1002/adma.201002689

[15] Zou M, Beckford S, Wei R, et al. Effects of surface roughness and energy on ice adhesion strength. Appl Surf Sci. 2011;257:3786–3792. Available from: http://www.sciencedirect.com/science/article/pii/S0169433210016727

[16] Alizadeh A, Yamada M, Li R, et al. Dynamics of ice nucleation on water repellent surfaces. Langmuir. 2012;28:3180–3186. Available from: http://dx.doi.org/10.1021/la2045256

[17] Guo P, Zheng Y, Wen M, et al. Icephobic/anti-icing properties of micro/nanostructured surfaces. Adv Mater. 2012;24:2642–2648. Available from: http://dx.doi.org/10.1002/adma.201104412

[18] Alizadeh A, Bahadur V, Kulkarni A, et al. Hydrophobic surfaces for control and enhancement of water phase transitions. MRS Bulletin. 2013;38:407–411.

[19] Eberle P, Tiwari MK, Maitra T, et al. Rational nanostructuring of surfaces for extraordinary icephobicity. Nanoscale. 2014;6:4874–4881. Available from: http://dx.doi.org/10.1039/C3NR06644D

[20] Schutzius TM, Jung S, Maitra T, et al. Physics of icing and rational design of surfaces with extraordinary icephobicity. Langmuir. 2015;31:4807–4821. Available from: http://dx.doi.org/10.1021/la502586a

[21] Sojoudi H, Wang M, Boscher ND, et al. Durable and scalable icephobic surfaces: similarities and distinctions from superhydrophobic surfaces. Soft Matter. 2016;12:1938–1963. Available from: http://dx.doi.org/10.1039/C5SM02295A

[22] He M, Wang J, Li H, et al. Super-hydrophobic surfaces to condensed micro-droplets at temperatures below the freezing point retard ice/frost formation. Soft Matter. 2011;7:3993–4000. Available from: http://dx.doi.org/10.1039/C0SM01504K

[23] Boinovich L, Emelyanenko AM, Korolev VV, et al. Effect of wettability on sessile drop freezing: when superhydrophobicity stimulates an

extreme freezing delay. Langmuir. 2014;30:1659–1668. Available from: http://dx.doi.org/10.1021/la403796g
[24] Hao P, Lv C, Zhang X. Freezing of sessile water droplets on surfaces with various roughness and wettability. Appl Phys Lett. 2014;104:161609. Available from: http://scitation.aip.org/content/aip/journal/apl/104/16/10.1063/1.4873345
[25] Wen M, Wang L, Zhang M, et al. Antifogging and icing-delay properties of composite micro- and nanostructured surfaces. ACS Appl Mater Interfaces. 2014;6:3963–3968. Available from: http://dx.doi.org/10.1021/am405232e
[26] Mishchenko L, Hatton B, Bahadur V, et al. Design of ice-free nanostructured surfaces based on repulsion of impacting water droplets. ACS Nano. 2010;4:7699–7707. Available from: http://dx.doi.org/10.1021/nn102557p
[27] Bahadur V, Mishchenko L, Hatton B, et al. Predictive model for ice formation on superhydrophobic surfaces. Langmuir. 2011;27:14143–14150. Available from: http://dx.doi.org/10.1021/la200816f
[28] Bird JC, Dhiman R, Kwon HM, et al. Reducing the contact time of a bouncing drop. Nature. 2013;503:385–388. Available from: http://dx.doi.org/10.1038/nature12740
[29] Liu Y, Moevius L, Xu X, et al. Pancake bouncing on superhydrophobic surfaces. Nat Phys. 2014;10:515–519. Available from: http://dx.doi.org/10.1038/nphys2980
[30] Maitra T, Tiwari MK, Antonini C, et al. On the nanoengineering of superhydrophobic and impalement resistant surface textures below the freezing temperature. Nano Lett. 2014;14:172–182. Available from: http://dx.doi.org/10.1021/nl4037092
[31] Ramachandran R, Sobolev K, Nosonovsky M. Dynamics of droplet impact on hydrophobic/icephobic concrete with the potential for superhydrophobicity. Langmuir. 2015;31:1437–1444. Available from: http://dx.doi.org/10.1021/la504626f
[32] Farhadi S, Farzaneh M, Kulinich S. Anti-icing performance of superhydrophobic surfaces. Appl Surf Sci. 2011;257:6264–6269. Available from: http://www.sciencedirect.com/science/article/pii/S0169433211002480
[33] Bengaluru Subramanyam S, Kondrashov V, Rühe J, et al. Low ice adhesion on nano-textured superhydrophobic surfaces under supersaturated conditions. ACS Appl Mater Interfaces. 2016;8:12583–12587. Available from: http://dx.doi.org/10.1021/acsami.6b01133
[34] Chen J, Liu J, He M, et al. Superhydrophobic surfaces cannot reduce ice adhesion. Appl Phys Lett. 2012;101:111603. Available from: https://doi.org/10.1063/1.4752436
[35] Kulinich SA, Farhadi S, Nose K, et al. Superhydrophobic surfaces: are they really ice-repellent?Langmuir. 2011;27:25–29. Available from: http://dx.doi.org/10.1021/la104277q
[36] Nosonovsky M, Hejazi V. Why superhydrophobic surfaces are not always icephobic. ACS Nano. 2012;6:8488–8491. Available from: http://dx.doi.org/10.1021/nn302138r
[37] Stone HA. Ice-phobic surfaces that are wet. ACS Nano. 2012;6:6536–6540. Available from: http://dx.doi.org/10.1021/nn303372q
[38] Varanasi KK, Deng T, Smith JD, et al. Frost formation and ice adhesion on superhydrophobic surfaces. Appl Phys Lett. 2010;97:234102. Available from: https://doi.org/10.1063/1.3524513
[39] Quéré D. Non-sticking drops. Rep Prog Phys. 2005;68:2495. Available from: http://stacks.iop.org/0034-4885/68/i=11/a=R01
[40] Solomon BR, Subramanyam SB, Farnham TA, et al. Non-wettable surfaces: theory, preparation and applications. Cambridge: The Royal Society of Chemistry; 2017. Chapter 10, Lubricant-impregnated surfaces; p. 285–318. Available from: http://dx.doi.org/10.1039/9781782623953-00285
[41] Stamatopoulos C, Hemrle J, Wang D, et al. Exceptional anti-icing performance of self-impregnating slippery surfaces. ACS Appl Mater Interfaces. 2017;9:10233–10242. Available from: http://dx.doi.org/10.1021/acsami.7b00186
[42] Wong TS, Kang SH, Tang SKY, et al. Bioinspired self-repairing slippery surfaces with pressure-stable omniphobicity. Nature. 2011;477:443–447. Available from: http://www.nature.com/nature/journal/v477/n7365/abs/nature104 47.html
[43] Kim P, Wong TS, Alvarenga J, et al. Liquid-infused nanostructured surfaces with extreme anti-ice and anti-frost performance. ACS Nano. 2012;6:6569–6577. Available from: http://dx.doi.org/10.1021/nn302310q
[44] Wilson PW, Lu W, Xu H, et al. Inhibition of ice nucleation by slippery liquid-infused porous surfaces (slips). Phys Chem Chem Phys. 2013;15:581–585. Available from: http://dx.doi.org/10.1039/C2CP43586A
[45] Anand S, Paxson AT, Dhiman R, et al. Enhanced condensation on lubricant-impregnated nanotextured surfaces. ACS Nano. 2012;6:10122–10129. Available from: http://dx.doi.org/10.1021/nn303867y
[46] Rykaczewski K, Anand S, Subramanyam SB, et al. Mechanism of frost formation on lubricant-impregnated surfaces. Langmuir. 2013;29:5230–5238. Available from: http://dx.doi.org/10.1021/la400801s
[47] Smith JD, Dhiman R, Anand S, et al. Droplet mobility on lubricant-impregnated surfaces. Soft Matter. 2013;9:1772–1780. Available from: http://dx.doi.org/10.1039/C2SM27032C
[48] Yin X, Zhang Y, Wang D, et al. Integration of self-lubrication and near-infrared photothermogenesis for excellent anti-icing/deicing performance. Adv Funct Mater. 2015;25:4237–4245. Available from: http://dx.doi.org/10.1002/adfm.201501101
[49] Yeong YH, Wang C, Wynne KJ, et al. Oil-infused superhydrophobic silicone material for low ice adhesion with long-term infusion stability. ACS Appl Mater Interfaces. 2016;8:32050–32059. Available from: http://dx.doi.org/10.1021/acsami.6b11184
[50] Subramanyam SB, Rykaczewski K, Varanasi KK. Ice adhesion on lubricant-impregnated textured surfaces. Langmuir. 2013;29:13414–13418. Available from: http://dx.doi.org/10.1021/la402456c
[51] Molinero V, Moore EB. Water modeled as an intermediate element between carbon and silicon. J Phys Chem B. 2009;113:4008–4016. Available from: http://dx.doi.org/10.1021/jp805227c
[52] Moore EB, de la Llave E, Welke K, et al. Freezing, melting and structure of ice in a hydrophilic nanopore. Phys Chem Chem Phys. 2010;12:4124–4134. Available from: http://dx.doi.org/10.1039/B919724A
[53] Moore EB, Molinero V. Structural transformation in supercooled water controls the crystallization rate of ice. Nature. 2011;479:506–508. Available from: http://www.nature.com/nature/journal/v479/n7374/abs/nature10586.html
[54] Moore EB, Molinero V. Ice crystallization in water's "no-man's land". J Chem Phys. 2010;132:244504. Available from: http://scitation.aip.org/content/aip/journal/jcp/132/24/10.1063/1.3451112
[55] Lupi L, Hudait A, Molinero V. Heterogeneous nucleation of ice on carbon surfaces. J Am Chem Soc. 2014;136:3156–3164. Available from: http://dx.doi.org/10.1021/ja411507a
[56] Reinhardt A, Doye JPK. Free energy landscapes for homogeneous nucleation of ice for a monatomic water model. J Chem Phys. 2012;136:054501. Available from: http://scitation.aip.org/content/aip/journal/jcp/136/5/10.1063/1.3677192
[57] Hudait A, Molinero V. Ice crystallization in ultrafine water–salt aerosols: nucleation, ice-solution equilibrium, and internal structure. J Am Chem Soc. 2014;136:8081–8093. Available from: http://dx.doi.org/10.1021/ja503311r
[58] Li T, Donadio D, Galli G. Ice nucleation at the nanoscale probes no man's land of water. Nat Commun. 2013;4:1887.
[59] Bullock G, Molinero V. Low-density liquid water is the mother of ice: on the relation between mesostructure, thermodynamics and ice crystallization in solutions. Faraday Discuss. 2013;167:371–388. Available from: http://dx.doi.org/10.1039/C3FD00085K
[60] Haji-Akbari A, DeFever RS, Sarupria S, et al. Suppression of sub-surface freezing in free-standing thin films of a coarse-grained model of water. Phys Chem Chem Phys. 2014;16:25916–25927. Available from: http://dx.doi.org/10.1039/C4CP03948C
[61] Singh JK, Müller-Plathe F. On the characterization of crystallization and ice adhesion on smooth and rough surfaces using molecular dynamics. Appl Phys Lett. 2014;104:021603. Available from: http://scitation.aip.org/content/aip/journal/apl/104/2/10.106 3/1.4862257
[62] Fitzner M, Sosso GC, Cox SJ, et al. The many faces of heterogeneous ice nucleation: interplay between surface morphology and

hydrophobicity. J Am Chem Soc. 2015;137:13658–13669. Available from: http://dx.doi.org/10.1021/jacs.5b08748
[63] Cox SJ, Kathmann SM, Slater B, et al. Molecular simulations of heterogeneous ice nucleation. I. Controlling ice nucleation through surface hydrophilicity. J Chem Phys. 2015;142:184704. Available from: http://scitation.aip.org/content/aip/journal/jcp/142/18/10.10 63/1.4919714
[64] Qiu Y, Odendahl N, Hudait A, et al. Ice nucleation efficiency of hydroxylated organic surfaces is controlled by their structural fluctuations and mismatch to ice. J Am Chem Soc. 2017;139:3052–3064. Available from: http://dx.doi.org/10.1021/jacs.6b12210
[65] Cui S, Siepmann J, Cochran H, et al. Intermolecular potentials and vapor–liquid phase equilibria of perfluorinated alkanes. Fluid Phase Equilib. 1998;146:51–61. Available from: http://www.sciencedirect.com/science/article/pii/S0378381298002167
[66] Cornell WD, Cieplak P, Bayly CI, et al. A second generation force field for the simulation of proteins, nucleic acids, and organic molecules. J Am Chem Soc. 1995;117:5179–5197. Available from: http://dx.doi.org/10.1021/ja00124a002
[67] Jorgensen WL, Maxwell DS, Tirado-Rives J. Development and testing of the opls all-atom force field on conformational energetics and properties of organic liquids. J Am Chem Soc. 1996;118:11225–11236. Available from: http://dx.doi.org/10.1021/ja9621760
[68] Canongia Lopes JN, Deschamps J, Pádua AAH. Modeling ionic liquids using a systematic all-atom force field. J Phys Chem B. 2004;108:2038–2047. Available from: http://dx.doi.org/10.1021/jp0362133
[69] Singh JK, Kofke DA, Errington JR. Surface tension and vapor–liquid phase coexistence of the square-well fluid. J Chem Phys. 2003;119:3405–3412. Available from: https://doi.org/10.1063/1.1590313
[70] Singh JK, Kofke DA. Molecular simulation study of the effect of pressure on the vapor–liquid interface of the square-well fluid. Langmuir. 2005;21:4218–4226. Available from: https://doi.org/10.1021/la0471947
[71] Qiu Y, Molinero V. Morphology of liquid–liquid phase separated aerosols. J Am Chem Soc. 2015;137:10642–10651. Available from: http://dx.doi.org/10.1021/jacs.5b05579
[72] Katiyar P, Singh JK. A coarse-grain molecular dynamics study of oil–water interfaces in the presence of silica nanoparticles and nonionic surfactants. J Chem Phys. 2017;146:204702. Available from: https://doi.org/10.1063/1.4984073
[73] Dutta RC, Khan S, Singh JK. Wetting transition of water on graphite and boron-nitride surfaces: a molecular dynamics study. Fluid Phase Equilib. 2011;302:310–315. Available from: http://www.sciencedirect.com/science/article/pii/S0378381210003663
[74] Metya AK, Khan S, Singh JK. Wetting transition of the ethanol–water droplet on smooth and textured surfaces. J Phys Chem C. 2014;118:4113–4121. Available from: http://dx.doi.org/10.1021/jp4096437
[75] Cheng A, Steele WA. Computer simulation of ammonia on graphite. I. Low temperature structure of monolayer and bilayer films. J Chem Phys. 1990;92:3858–3866. Available from: https://doi.org/10.1063/1.458562
[76] Plimpton S. Fast parallel algorithms for short-range molecular dynamics. J Comput Phys. 1995;117:1–19. Available from: http://www.sciencedirect.com/science/article/pii/S002199918571039X
[77] Grubmüller H, Heymann B, Tavan P. Ligand binding: molecular mechanics calculation of the streptavidin-biotin rupture force. Science. 1996;271:997–999. Available from: http://science.sciencemag.org/content/271/5251/997
[78] Jarzynski C. Nonequilibrium equality for free energy differences. Phys Rev Lett. 1997 Apr;78:2690–2693. Available from: https://link.aps.org/doi/10.1103/PhysRevLett.78.2690
[79] Izrailev S, Stepaniants S, Balsera M, et al. Molecular dynamics study of unbinding of the avidin-biotin complex. Biophys J. 1997;72:1568–1581. Available from: http://www.sciencedirect.com/science/article/pii/S0006349597788040
[80] Park S, Khalili-Araghi F, Tajkhorshid E, et al. Free energy calculation from steered molecular dynamics simulations using Jarzynski's equality. J Chem Phys. 2003;119:3559–3566. Available from: https://doi.org/10.1063/1.1590311
[81] Park S, Schulten K. Calculating potentials of mean force from steered molecular dynamics simulations. J Chem Phys. 2004;120:5946–5961. Available from: https://doi.org/10.1063/1.1651473
[82] Xia W, Hsu DD, Keten S. Dependence of polymer thin film adhesion energy on cohesive interactions between chains. Macromolecules. 2014;47:5286–5294. Available from: http://dx.doi.org/10.1021/ma5006974
[83] Xiao S, He J, Zhang Z. Nanoscale deicing by molecular dynamics simulation. Nanoscale. 2016;8:14625–14632. Available from: http://dx.doi.org/10.1039/C6NR02398C
[84] Bao L, Huang Z, Priezjev NV, et al. A significant reduction of ice adhesion on nanostructured surfaces that consist of an array of single-walled carbon nanotubes: a molecular dynamics simulation study. Appl Surf Sci. 2018;437:202–208. Available from: https://www.sciencedirect.com/science/article/pii/S016943321733684X
[85] Kreder MJ, Alvarenga J, Kim P, et al. Design of anti-icing surfaces: smooth, textured or slippery? Nat Rev Mater. 2016;1:15003. Available from: http://dx.doi.org/10.1038/natrevmats.2015.3